UCLA
UCLA Previously Published Works

Title

Interaction of ions, atoms, and small molecules with quantized vortex lines in superfluid ^{4}He

Permalink

https://escholarship.org/uc/item/8zm0k4xb

Journal

Journal of Chemical Physics, 142(6)

ISSN

0021-9606

Authors

Mateo, D
Eloranta, J
Williams, GA

Publication Date

2015-02-14

DOI

10.1063/1.4907597

Peer reviewed

eScholarship.org Powered by the California Digital Library
University of California

Interaction of ions, atoms, and small molecules with quantized vortex lines in superfluid ^{4}He

David Mateo, Jussi Eloranta, and Gary A. Williams

Citation: The Journal of Chemical Physics **142**, 064510 (2015); doi: 10.1063/1.4907597
View online: https://doi.org/10.1063/1.4907597
View Table of Contents: http://aip.scitation.org/toc/jcp/142/6
Published by the American Institute of Physics

Articles you may be interested in

Dynamics of vortex assisted metal condensation in superfluid helium
The Journal of Chemical Physics **138**, 204307 (2013); 10.1063/1.4807382

Theoretical modeling of electron mobility in superfluid ^{4}He
The Journal of Chemical Physics **145**, 044105 (2016); 10.1063/1.4959293

Note: A latched comparator circuit for triggering continuous-wave cavity ring-down spectroscopy
Review of Scientific Instruments **84**, 066109 (2013); 10.1063/1.4811846

First-principle optimal local pseudopotentials construction via optimized effective potential method
The Journal of Chemical Physics **144**, 134108 (2016); 10.1063/1.4944989

Time-resolved study of laser initiated shock wave propagation in superfluid ^{4}He
The Journal of Chemical Physics **145**, 124504 (2016); 10.1063/1.4963097

Soliton propagation on vortex cores and the Hasimoto soliton
The Physics of Fluids **26**, 3173 (1983); 10.1063/1.864088

Interaction of ions, atoms, and small molecules with quantized vortex lines in superfluid ^{4}He

David Mateo,[1] Jussi Eloranta,[1,a)] and Gary A. Williams[2]
[1]*Department of Chemistry and Biochemistry, California State University at Northridge, 18111 Nordhoff St., Northridge, California 91330, USA*
[2]*Department of Physics and Astronomy, University of California, Los Angeles, California 90095, USA*

(Received 17 December 2014; accepted 26 January 2015; published online 10 February 2015)

The interaction of a number of impurities (H_2, Ag, Cu, Ag_2, Cu_2, Li, He_3^+, He^* (^3S), He_2^* ($^3\Sigma_u$), and e^-) with quantized rectilinear vortex lines in superfluid ^{4}He is calculated by using the Orsay-Trento density functional theory (DFT) method at 0 K. The Donnelly-Parks (DP) potential function binding ions to the vortex is combined with DFT data, yielding the impurity radius as well as the vortex line core parameter. The vortex core parameter at 0 K (0.74 Å) obtained either directly from the vortex line geometry or through the DP potential fitting is smaller than previously suggested but is compatible with the value obtained from re-analysis of the Rayfield-Reif experiment. All of the impurities have significantly higher binding energies to vortex lines below 1 K than the available thermal energy, where the thermally assisted escape process becomes exponentially negligible. Even at higher temperatures 1.5-2.0 K, the trapping times for larger metal clusters are sufficiently long that the previously observed metal nanowire assembly in superfluid helium can take place at vortex lines. The binding energy of the electron bubble is predicted to decrease as a function of both temperature and pressure, which allows adjusting the trap depth for either permanent trapping or to allow thermally assisted escape. Finally, a new scheme for determining the trapping of impurities on vortex lines by optical absorption spectroscopy is outlined and demonstrated for He^*. © *2015 AIP Publishing LLC.* [http://dx.doi.org/10.1063/1.4907597]

I. INTRODUCTION

A wealth of experimental studies has been devoted to studying the interaction of ions and small molecules with quantized vortex lines in bulk superfluid helium.[1,2,2–17] The interaction of electrons with quantized vortex lines was first observed in experiments by Careri *et al.* where the ion current was strongly attenuated along the direction perpendicular to the vortex lines.[1] This observation is consistent with the interpretation that electrons are captured and retained by vortex lines until they escape via a thermally assisted process.[18] Analogous experiments were also carried out for positive ions showing a similar behavior except that its interaction with vortices appeared to be smaller than for the electron.[8–10] By orienting the collecting electric field parallel to the axis of rotation, it was also possible to study charge mobility along the vortex lines, which was generally observed to be lower than for the free ion.[2,4,17] The interaction of ions with vortex waves and rotons has been proposed to be responsible for the observed reduction in mobility.[3,5] Nucleation of vortex rings during ion transport above some critical threshold velocity has also been studied experimentally but there appears to be no general consensus on the exact microscopic processes leading to such behavior and it is more difficult to relate these experiments to the impurity–vortex binding energies.[17]

Since these pioneering studies, many experimental techniques have taken advantage of the significant binding energy of impurities towards vortex lines. For example, the first experiment displaying spatially resolved photographs of vortex arrays formed in rotating superfluid helium was based on seeding vortex lines with electrons and subsequently transporting them along the vortices for imaging.[11,19] More recently, ballistic neutral He_2^* excimer molecules have been used to study the interaction of these heliophobic species with vortex tangles (i.e., quantum turbulence) and fluorescence imaging using these molecules as probes has been suggested as a way to visualize vortex lines.[6,20,21] Light scattering by solid hydrogen particles trapped on vortex lines has also been successfully used to visualize vortex lines as well as the vortex line reconnect events followed by the emission of Kelvin waves.[12,22] Finally, this concept was also used recently to seed vortex lines with metal atoms and clusters that were produced by laser ablation.[15,16,23–26] This process was shown to lead to the formation of one dimensional metallic nanowires in a complex network. Similar behavior has also been observed in ^{4}He droplets where metal nanowires were shown to nucleate on vortex lines.[27–30]

In the low temperature regime, all these phenomena are ultimately dictated by the impurity–vortex line potential, which depends on the impurity–superfluid helium interaction, the impurity impact velocity on the vortex line, and the vortex line geometry itself. In this work, we assume that the vortex line remains rectilinear in interacting with the impurity (i.e., rigid geometry) and ignore the possible energy

a)E-mail: Jussi.Eloranta@csun.edu.

 © 2015 AIP Publishing LLC

dissipation channels that can lead to the creation of, for example, vortex waves.[31] Within these assumptions, the impurity–vortex distance can be defined exactly and the corresponding interaction energy be calculated by vortex hydrodynamics,[17,32,33]

$$E_{IM-Vortex} = -\frac{1}{2}\int \rho_s(r)|v_s(r)|^2 d^3r, \tag{1}$$

where ρ_s denotes the superfluid density around the impurity and v_s denotes the velocity field associated with the quantized vortex line. This classical expression accounts for the loss of kinetic energy due to the liquid displaced by the impurity. Within the Gross-Pitaevskii (GP) theory, which assumes a dilute Bose gas, approximate functional forms for both ρ_s and v_s around a rectilinear vortex line have been proposed by Fetter[34] and applied to describe vortex lines in superfluid helium by Parks and Donnelly,[32]

$$\rho_s(r) = \rho_{s,0}\frac{r^2}{r^2 + a_F^2} \quad \text{and} \quad |v_s(r)| = \frac{\hbar}{m_{He} r}, \tag{2}$$

where $\rho_{s,0}$ corresponds to superfluid helium bulk density (e.g., $\rho_{s,0} = 0.021836$ Å^{-3} at 0 K), a_F is the healing length compatible with this expression, and m_{He} is helium atom mass. Since we apply Eq. (2) to describe superfluid helium rather than a dilute Bose gas, we denote the healing length in this expression by a_F to emphasize that this is an effective value that will reproduce the approximate liquid density profile around a vortex line. The value of a_F is expected to be of similar order as the vortex core parameter defined by the hollow core model.[35,36] When analyzing impurity–vortex interactions, the value for the vortex core parameter has been typically obtained from the Rayfield-Reif experiment as 1.20–1.46 Å near 0 K[32,37] and the current recommended value is 1.28 ± 0.13 Å at 0.28 K.[17,36,38] However, more recently, Glaberson and Donnelly re-analyzed the Rayfield-Reif experiment and obtained a considerably smaller value for the vortex core parameter, 0.81 Å.[39] In general, all these values are smaller than predicted by the GP theory at 0 K where $a_F = 1.4$ Å (see GP data in Fig. 1).[34] The only remaining parameter in Eq. (2), the bulk liquid superfluid density, $\rho_{s,0}$, is well-known as a function of temperature and pressure.[40]

The temperature dependence of the superfluid helium healing length a has been typically expressed in terms of the following empirical power-law:[36]

$$a(T) = a(0)\left(\frac{T_\lambda}{T_\lambda - T}\right)^\nu, \tag{3}$$

where $a(0)$ is the 0 K value for the healing length, T_λ is the helium lambda transition temperature (2.176 K at saturated vapor pressure), T is the liquid temperature (K), and ν is an empirical exponent. The GP theory predicts $\nu = 1/2$, whereas experiments suggest $\nu = 2/3$.[36,41] In general, however, there appears to be a large discrepancy between the theoretical and experimental estimates for $a(0)$, which differ from each other by a factor of two or even more.[41]

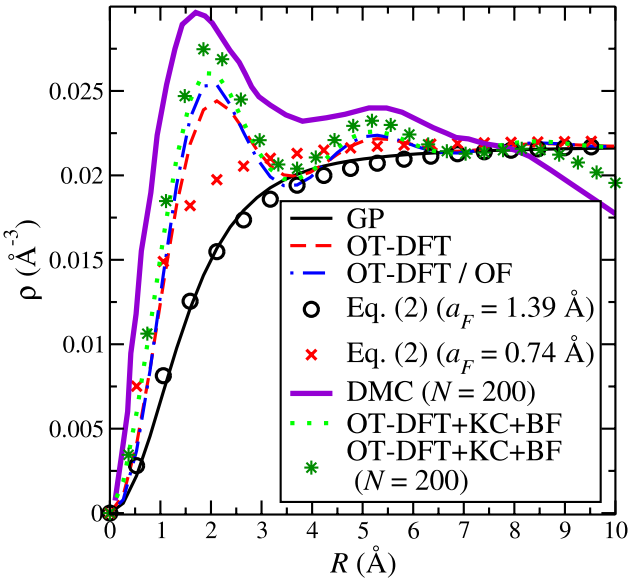

FIG. 1. Theoretical liquid density profiles along the coordinate perpendicular to a rectilinear vortex line. GP denotes the Gross-Pitaevskii theory for superfluid helium (this work), OT-DFT is the Orsay-Trento DFT (KC: with the kinetic energy correlation functional included; BF: the backflow functional included), OF indicates that the vortex was obtained by using the Onsager-Feynman ansatz,[53,54] and DMC corresponds to diffusion Monte Carlo calculations of Boronat *et al.*[50] All calculations refer to bulk liquid unless the droplet size N is indicated (droplet surface not shown). The open circles and crosses correspond to least squares fits of Eq. (2) to the GP and OT-DFT results, respectively. The resulting values for parameter a_F are shown in the caption.

Following Parks and Donnelly, the vortex–impurity interaction potential can be evaluated by integrating Eq. (1),[32]

$$V_{IM-Vortex}(r) = -2\pi\rho_{s,0}\left(\frac{\hbar^2}{m_{He}}\right)^2 \times \int_0^R \frac{\left(R^2 - \xi^2\right)^{1/2}\xi}{\left[\left(\xi^2 + r^2 + a_F^2\right)^2 - 4r^2\xi^2\right]^{1/2}} d\xi, \tag{4}$$

where R is the classical radius for a spherical impurity (i.e., interface profile described by a Heaviside function) and r is the vortex–impurity distance. This expression accounts for the hydrodynamic Bernoulli interaction between a particle occupying a given volume in the liquid and a classical vortex line.[17,32] In addition to the known temperature dependence in $\rho_{s,0}$,[40] a_F is also expected to be temperature dependent as suggested by Eq. (3).

In this paper, we apply bosonic density functional theory (DFT) to obtain the vortex core structure, solvation structures for selected impurities (H_2, Ag, Cu, Ag_2, Cu_2, Li, He_3^+, He^* (^3S), He_2^* ($^3\Sigma_u$), and e^-) and calculate the vortex–impurity interaction energy profiles assuming a rigid rectilinear vortex line structure. These results are compared with the Parks-Donnelly form given by Eq. (4), and new parametrizations for all the considered impurities are given. The relationship between a_F and other commonly used parameters to describe the vortex line radius as well as the various ways of defining the impurity solvation cavity radii is discussed based on the calculated liquid density profiles. Thermal corrections to both $\rho_{s,0}$ and a_F are considered for the solvated electron for

which experimental results were previously obtained in the temperature range of 1.5–1.8 K.

II. THEORY

Superfluid ^{4}He was modeled by the Orsay-Trento DFT (OT-DFT),[42–44] and the interaction with guest ions/atoms/molecules was included by convoluting the liquid and impurity densities with the corresponding pair potential. The present treatment includes also the zero-point response of the guest by solving the following coupled non-linear time-dependent Schrödinger equations:[33,45]

$$i\hbar\frac{\partial\Psi(r,t)}{\partial t} = -\frac{\hbar^2}{2m_{He}}\Delta\Psi(r,t) + V_{OT}[\Psi]\,\psi(r,t) + \int |\psi(r',t)|^2 V_{IM}(|r-r'|)d^3r' \times \Psi(r,t), \quad (5)$$

$$i\hbar\frac{\partial\psi(r,t)}{\partial t} = -\frac{\hbar^2}{2m_{IM}}\Delta\psi(r,t) + \int |\Psi(r',t)|^2 \times V_{IM}(|r-r'|)d^3r' \times \psi(r,t)$$

in imaginary time (i.e., $t = i\tau$), where $\Psi(r,t)$ is the liquid order parameter, $\psi(r,t)$ is the impurity wavefunction, V_{OT} is the functional derivative of the OT energy functional with respect to the complex conjugate of the order parameter,[43] V_{IM} represents the impurity–helium pair interaction, and m_{IM} is the impurity mass. For other than the electron, this treatment neglects the liquid–impurity correlation, which could slightly reduce the impurity solvation cavity size for light impurities (e.g., H_2). The backflow and kinetic energy correlation terms were not included in the OT functional unless explicitly noted. The contribution of the kinetic energy correlation term to the binding energies was estimated to be about 1 K. For atomic/molecular impurities, V_{IM} simply corresponds to the pair-potential,[15,46,47] whereas for the electron, it also includes the short-range correlation effects.[48] In order to compute the interaction between a rectilinear vortex line located at $z = 0$ and a given impurity fixed on the x-axis, their positions must be constrained during the calculation. For the vortex line, this is achieved by including an additional penalty term in Eq. (5), which requires $\Psi \equiv 0$ along the core. For the impurity wavefunction, the following penalty term was included in the potential (vortex–impurity coordinate along x; $r = (x, y, z)$):

$$V'(\psi, r, t) = 2\alpha\,(x - x_0)\int \psi(r',t)^*\,(x' - x_0)\,\psi(r',t)d^3r', \quad (6)$$

where the constraint amplitude $\alpha \approx 10^{-5}$ a.u. and x_0 is the constrained vortex–impurity position on the x-axis. The contribution of Eq. (6) was subtracted from the total energy calculation.

In order to converge to the lowest vortex state solution, an initial guess for the order parameter was constructed according to the previously described approach.[33] This functional form is orthogonal to the ground state liquid solution, and therefore, convergence of the imaginary time propagation becomes constrained to the lowest vortex state solution.[44] The Neumann boundary condition employed in the calculations is not fully compatible with the vortex solution at the simulation box corners, but the distortion caused by the boundaries was negligible for the simulation box sizes used in this study.

The details for the numerical solution of Eq. (5) are given elsewhere.[43] Both the order parameter and the impurity wavefunctions were represented by $512 \times 256 \times 256$ Cartesian grids with a 0.5 Å spatial step. For imaginary time calculations, the applied time step was 20 fs with typically 5000 steps executed to reach proper convergence. The total energy corresponding to Eq. (5) was calculated by numerically integrating the resulting energy density, which was also used to monitor the convergence of the imaginary time process. The resulting impurity–vortex interaction energies as a function of distance were fitted to Eq. (4) using the non-linear least squares method (the Levenberg-Marquardt algorithm, LMDIF in Minpack[49]). Equation (4) itself was integrated numerically to obtain $V_{IM-Vortex}(r)$ at the required values of r. The total binding energy provided by this potential (i.e., $r = 0$) can be calculated analytically from

$$V_{IM-Vortex}(0) = 2\pi\rho_{s,0}\left(\frac{\hbar}{m_{He}}\right)^2\left[\frac{\sqrt{R^2+a_F^2}}{2} \times \ln\left(\frac{a_F^2 + 2R^2 - 2R\sqrt{R^2+a_F^2}}{a_F^2}\right) + R\right] \quad (7)$$

which includes two free parameters R and a_F. Note that if the value of a_F is constant (i.e., independent of R but could still depend on temperature), Eq. (7) can be used to relate the experimentally obtained binding energies directly to the impurity radii in the liquid. The values of R and a_F are specific to the temperature and pressure where the experiment was carried out.

III. RESULTS AND DISCUSSION

A comparison between previous diffusion Monte Carlo (DMC) calculations[50] and the present OT-DFT calculations for the radial superfluid density distribution around a rectilinear vortex line in a small helium droplet ($N = 200$) is shown in Fig. 1. Despite the small differences in the curvature near the vortex core and the maximum liquid density value reached, both methods produce comparable radial extents for the vortex line. The construction of the vortex phase winding within a single order parameter implies that the density at the center of the vortex must be zero. This is consistent with the previously mentioned DMC data but disagrees with another set of quantum Monte Carlo calculations employing a different technique.[51,52] At present, it appears that this problem, whether the vortex core is completely empty or not, seems to be still unsettled, so we have to bear in mind that this issue could also affect the vortex–impurity binding energies to some extent. On increasing the droplet size, the vortex diameter remains very similar all the way to the bulk superfluid helium limit as demonstrated in Fig. 1. The inclusion of the kinetic energy correlation and backflow terms in OT-DFT increases the maximum density next to the vortex core only slightly, which indicates that these terms can be neglected in the present

study (see also Ref. 33). Finally, to demonstrate the difference between the OT-DFT and GP theory results, the corresponding liquid densities are also included in Fig. 1. The GP model yields a noticeably larger vortex core size than both DMC and OT-DFT and it is, therefore, a rather poor model to describe vortex lines in superfluid helium.

We have also verified that the present method of calculating the vortex line structure (i.e., including the real phase winding in order parameter) gives essentially the same liquid density profile as obtained by the previously applied Onsager-Feynman (OF) potential approach (cf. Fig. 1).[15,54] As the OF potential does not include the phase winding explicitly, the calculations employing this approach tend to converge much faster and do not require any special consideration for the boundary condition. Within the OF ansatz, the vortex contribution to the total energy appears in the form of potential energy. For this reason, the kinetic energy originating from the phase circulation and the potential energy from the OF potential represent the same interaction. This implies that, in fact, the "static binding" and "Bernoulli interaction" introduced in Ref. 15 represent the same contribution and should not both be included at the same time when calculating the total energy.

The vortex core size is often discussed in terms of healing length (or vortex core parameter), a, which represents the vortex line radius in a model specific way. However, it is clear from Fig. 1 that it is not straight forward to define the geometric vortex radius exactly as the liquid density profile exhibits oscillations arising from the correlated nature of superfluid helium. The maximum in the liquid density near the vortex line appears to be around ≈2 Å but the liquid density first reaches the bulk level already at 1.4 Å. Note that the latter value is very close to the 0 K value for the vortex core parameter (1.3 Å) suggested by Vinen *et al.*[36] Thus, just like for solvated impurities in superfluid helium, there is some ambiguity in defining the object radius (for discussion on vortex and bubble radii, see Refs. 36 and 55). One way to define the vortex radius is to use Eq. (2) and the associated parameter a_F.[34] This approximate density profile form is able to describe the GP results (see Fig. 1) very well but it is unable to account for the oscillations present in the OT-DFT results. However, even in this case, it is able to follow the OT-DFT results such that it just effectively smooths out the oscillatory behavior (see Fig. 1). In this sense, the form of Eq. (2) is useful for representing superfluid helium density around vortex lines approximately with the value of a_F obtained through a least-squares fit of Eq. (4) to the OT-DFT data. It can be seen in Fig. 1 that the value of a_F is slightly less than the vortex interface barycenter, whereas the vortex core parameter (1.28 Å)[36] points to the opposite side of the barycenter. On the other hand, the new vortex core parameter value (0.81 Å), which was obtained by re-analyzing the Rayfield-Reif experiment,[39] appears to be very close to a_F obtained from Eq. (4) and OT-DFT at 0 K. Finally, we note that the GP model at 0 K yields approximately twice as large a value for a_F as compared to OT-DFT, which would, for example, significantly reduce the impurity–vortex binding energy provided by Eq. (4).

The present OT-DFT calculations were carried out at 0 K, but in order to compare with experimental data, it is necessary to extrapolate both $\rho_{s,0}$ and a_F to finite temperatures. Since it is apparent now that the vortex core parameter and a_F differ at most by the reference point for specifying the vortex radius, it is expected that they both follow the same temperature dependence as given by Eq. (3),

$$a_F(T) = a_F(0)\left(\frac{T_\lambda}{T_\lambda - T}\right)^{\nu}, \tag{8}$$

where the value of ν should be in the range of 1/2 - 2/3.[36,41] This equation predicts that a_F becomes larger when temperature is increased (i.e., the vortex core diameter increases). For example, this equation predicts that the value of a_F goes from ≈0.75 Å at 0 K to 1.5–1.8 Å at 1.6 K depending on the value of ν chosen. Finally, we note that the thermal OT-DFT model cannot reproduce the temperature dependence of a_F because it does not explicitly consider the thermally excited Kelvin waves on vortex lines that contribute to the radius.

Based on Eq. (7), the binding energy of an impurity to rectilinear vortex lines depends on both the impurity radius R, the vortex radius ($\approx a_F$) and the superfluid density $\rho_{s,0}$. All these parameters exhibit temperature dependence, which is relevant to the analysis of the experimental data. The two reference systems, for which the experimental vortex–impurity binding energies are available in the literature, are the positive and negative ions.[17] The positive ion (i.e., He_3^+; see Ref. 56) data were obtained between 0.28 K and 0.6 K, where both the baseline temperature correction and the temperature-dependent variation of these parameters within the measurement range can be largely neglected. As shown in Table I, the 0 K OT-DFT binding energy matches the experimentally obtained value closely (−16.0 K vs. −17.5 K).[7,13,17] The radius R based on Eq. (4) for the positive ion (see Table I) is $R \approx 6$ Å, which is consistent with the Atkins' snowball model.[17,57] As discussed in Ref. 56, the radius of the first solvation shell appears around 3.4 Å and the second shell near 6 Å. In that study, it was shown that the effective size for the positive ion corresponds to the first (solid) solvation shell whereas the ion size R extracted from the impurity–vortex interaction here apparently correlates with the secondary solvation shell position at ≈6 Å. This highlights that the experimentally determined impurity radii may strongly depend on the physical mechanism being considered. The measured low-temperature ion effective mass[58] of about 30 m_{He} also is evidence that the second solvation shell needs to be taken into account, since the first shell would give an effective mass of only about 18 m_{He}.[56]

It has been shown previously that the OT-DFT method combined with the He–electron pseudo-potential approach can be used to describe solvated electrons in superfluid helium with very good accuracy.[45,61] In particular, it was shown to reproduce the pressure dependence of the $1s - 1p$ and $1s - 2p$ optical transitions as a function of pressure very accurately. Therefore, the OT-DFT method can reliably model both vortex lines and solvated electrons. In order to compare the calculated 0 K electron–vortex binding energy to experimental data, it is necessary to consider the effect of the rather high temperature used in the experiments, 1.6–1.7 K. When analyzing the experimental data in this temperature interval,

TABLE I. Summary of impurity–vortex interaction parameters according to Eq. (4) at saturated vapor pressure and 0 K temperature where R represents the impurity radius according and a_F is the effective healing length. The approximate signs signify that R and a_F were estimated by fixing a_F to an average value obtained for the other similar "size" impurities and then using Eq. (7) to obtain the radius R that corresponds to $V_{IM-Vortex}(0)$ obtained from the OT-DFT calculation.

Impurity	R (Å)	a_F (Å)	OT-DFT $V_{IM-Vortex}(0)$ (K)	Exp. $V_{IM-Vortex}$ (K)
H_2 ($X\ ^1\Sigma_g$)	3.1	0.38	−9.4	...
Ag_2 ($X\ ^1\Sigma_g$)	3.9	0.51	−10.9	...
Cu_2 ($X\ ^1\Sigma_g$)	4.0	0.52	−11.4	...
Ag (^2S)	4.4	0.63	−12.0	...
Cu (^2S)	4.5	0.65	−12.5	...
He_3^+ ($X\ ^2\Sigma_g$)	≈5.7	≈0.75	−16.0	−17.5 at 0.28-0.6 K[7,13,17]
Li (^2S)	6.8	0.75	−21.5	...
He^* ($2s\ ^3S$)	7.1	0.77	−22.6	...
He_2^* ($a\ ^3\Sigma_u$)	8.6	0.80	−29.8	...
e^- ($1s$)	22.2	0.76	−109	−55 to −59 at 1.6 K[59,60]

the rather strong variation in $\rho_{s,0}$ as a function of temperature must be considered.[59] When this correction is included in the analysis, binding energies ranging from −55 K to −59.4 K are obtained.[59,60] This result is clearly far off from our 0 K OT-DFT value of −109 K, which, on the other hand, is also consistent with an earlier OT-DFT study (−104.5 K).[33] The superfluid fraction at 1.65 K is approximately 0.80 and the effective healing length is in the range of 1.5–1.9 Å (see Eq. (8); $a_F(0) = 0.76$ Å from Table I). Using these values to correct the 0 K OT-DFT result gives a binding energy of −67 K, which is already fairly close to the experimental value of −59.4 Å.[59] In order to consider the effect of temperature on R, we also applied the thermal OT-DFT model[62] to calculate the change in the binding energy (0 K vs. 1.6 K). As expected, the bubble radius decreases almost by 1 Å and the bubble interface geometry changes slightly. This, in turn, reduces the binding energy of the electron to the vortex line by 6 K, resulting in total binding energy of −61 K (vs. experimental range of −55 to −59.4 K). The analysis of the experimental results did not allow for the possibility of a temperature variation in a_F within the experimental interval (which is calculated to be ≈10%) and this may be one possible source for the remaining difference between the extrapolated OT-DFT and experimental values. Another thermally induced mechanism that could alternatively be responsible for reducing the electron–vortex interaction has been discussed previously in terms of temperature dependent local deformations of the vortex line induced by the impurity.[33,63] Both mechanisms (i.e., temperature dependence in a_F, $\rho_{s,0}$, and R and the vortex line deformation) predict similar magnitude corrections (ca. 30%) that reduce the 0 K binding energy close to the experimentally observed values at 1.6 K.[33] It seems clear that the temperature-dependent effects have to be taken into account, and so further including the vortex-deformation effect would seem to over-correct the binding energy to values below the experiments.

At temperatures below 1.5 K, the binding energy becomes quite large and the electrons should become permanently trapped on vortex lines. However, experiments in rotating pure ^{4}He showed that the trapping lifetime reached a maximum at 1.5 K and then began to decrease at lower temperatures.[11] It appears that this is a consequence of vortex motion induced by the lack of damping on the vortex cores as the normal fluid fraction is reduced at low temperatures. A charged line will lose its electrons if it encounters the walls of the confining bucket, and this became severe below 1 K where trapping times could be less than 10 s in small cells (but much longer in large cells where most lines are well away from the walls).[11,64] It was found that this loss of trapping in small cells could be overcome by adding ^{3}He to the ^{4}He, which provides frictional normal fluid even at very low temperatures; electrons could then be held at 0.07 K for many thousands of seconds in the experiment to image the vortices.[11,19] Further investigation of the trapping in ^{3}He-^{4}He mixtures showed that this was the unusual result of two separate changes induced by the ^{3}He in the ion-vortex system.[14] Below 1 K, the ^{3}He condenses onto the vortex core, which increases the core radius and greatly reduces the binding energy of positive ions to the point they can no longer be trapped.[13,14] Even the large electron bubbles are affected with lifetimes less than a few seconds at 0.4 K. Near 0.3 K and below, there is then a sudden change to the very long lifetime, as the ^{3}He apparently condenses onto the surface of the bubble, lowering the surface tension and increasing the bubble size. Unfortunately, neither of these effects can be easily modeled with the methods employed here because, at present, the suitable functionals for describing such mixed systems at finite temperatures have not yet been developed.[53,65]

The OT-DFT results for both positive and negative ion binding towards rectilinear vortex lines appear to be in good agreement with the experimentally observed values, demonstrating that the present theoretical method can reliably model such interactions. An overview of the calculated model parameters R and a_F at 0 K and saturated vapor pressure for Ag, Ag_2, Cu, Cu_2, H_2, Li, He^*, and He_2^* are given in Table I and the full interaction potential curves for selected species are plotted in Fig. 2. Previously, the attractive interaction between the aforementioned metal atoms and clusters with vortex lines was shown to lead to the formation of metal nanowire structures in superfluid helium.[15,16,23–26] The interaction of

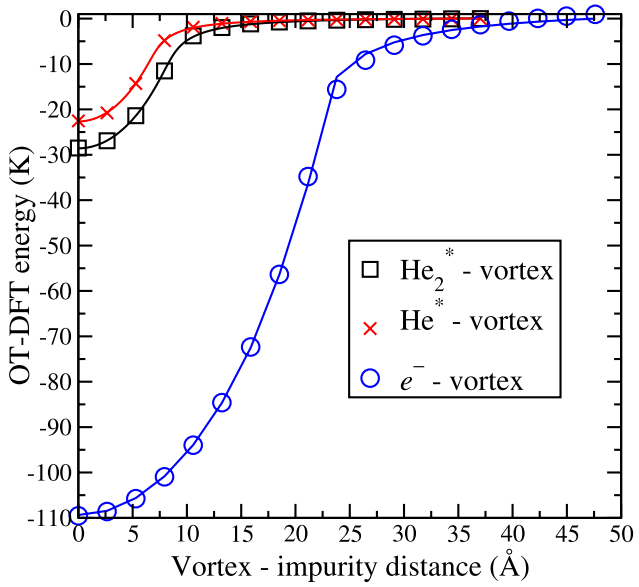

FIG. 2. The total OT-DFT energy at 0 K is plotted as a function of the vortex–impurity distance (discrete points) along with the least squares fit to Eq. (4) (continuous lines). The corresponding values for R and a_F are listed in Table I. The energy at the infinite distance limit was subtracted from the OT-DFT energies.

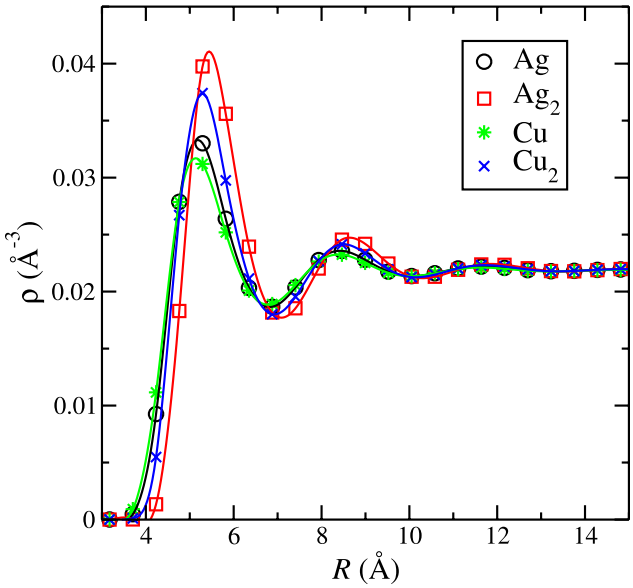

FIG. 3. Superfluid helium density around solvated Ag, Ag_2, Cu, and Cu_2 impurities at 0 K. The discrete points represent the DFT data whereas the continuous lines are obtained from cubic spline interpolation.

these species with rectilinear vortex lines was evaluated in Ref. 15 by the OF based OT-DFT method where the obtained binding energies have similar magnitudes as reported in this work. We should note, however, that apparently the limited simulation box size imposed by the computational resources available at the time leads to a distance dependent bias in the calculation of the total energy. This in turn was responsible for two artifacts in the calculated impurity–vortex interaction potentials, $V_{IM-Vortex}(r)$: (1) the shape of $V_{IM-Vortex}(r)$ was not given accurately at short distances and (2) impurities with large bubble radii displayed an energy barrier at the distance where the vortex line and the impurity came into contact. In agreement with that study, the present calculations confirm that both Ag and Cu atoms/clusters exhibit significant binding towards vortex lines (−11 K to −20 K; see Table I). This result is in line with the proposed mechanism for the nanowire formation where vortex lines act as templates for the assembly process.[15,16,23,26] As opposed to impurities residing in large bubbles ($R > 5$ Å), these atoms/dimers show reduced values for a_F indicating that an additional geometrical factor is incorporated in this parameter for small R. This may be in part due to the presence of a bound solvent layer around the impurity (see Fig. 3), which can be observed to play a role when comparing Cu vs. Cu_2 and Ag vs. Ag_2 data in Table I. In both cases, Eq. (4) predicts that the dimers have smaller value of R than the corresponding atoms but the inspection of OT-DFT density profiles shows exactly the opposite behavior. This can be traced down to the more pronounced first solvation shell structure around the dimers, which effectively introduces an energy tax and produces consequently smaller values for R and a_F. Molecular hydrogen shows the lowest binding towards vortex lines of the studied species (only −9 K).

Large hydrogen clusters, on the contrary, would show much larger binding towards vortex lines because the interaction increases approximately linearly as a function of the cluster radius (cf. Table I and Fig. 4). Note that for large clusters, the bubble radius becomes approximately equal to the cluster radius as the contribution of the bubble interface to the size becomes negligible. It should be noted, however, that this calculation neglects two important factors, which will eventually limit the binding energy for large impurities at finite temperatures. First, the present estimates apply to infinitely long rectilinear vortex lines and, by a simple geometrical argument, the binding towards small vortex rings must be limited by the length of the ring. Second, the phase evolution (and liquid circulation) becomes less and less pronounced far away from the vortex core and thermal perturbations

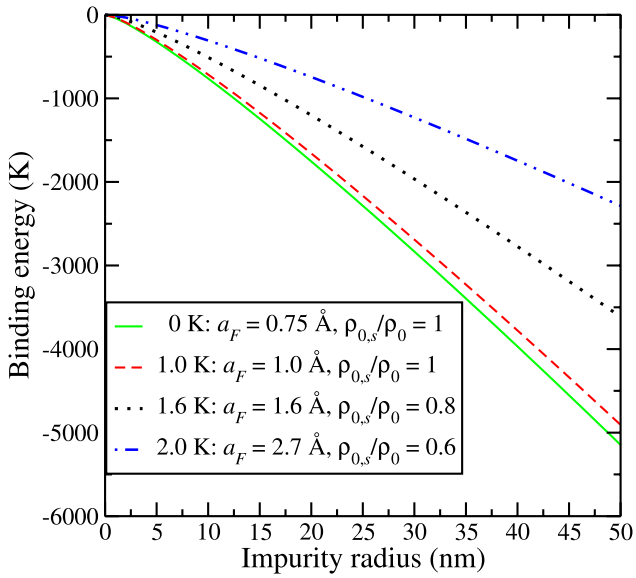

FIG. 4. Impurity–vortex binding energies according to Eq. (7) as a function of the impurity size at specified temperatures. Impurity size is assumed to be equal to the bubble radius R.

will eventually take over to randomize the phase there. This effectively limits the spatial extent of vorticity that can be "felt" by large impurities, placing an upper limit on the corresponding binding energy. Unfortunately, the present OT-DFT calculations cannot be used to assess such phase decoherence effects at finite temperatures. Despite of these limitations, large impurities are expected to trap on vortex lines efficiently, which allows their use, for example, to visualize vortex lines through light scattering.[12,66] Similar arguments can also be used for describing nanoparticle trapping on vortex lines[21] where the binding energy can be estimated by the same linear relationship. In an another line of experiments, trapping of molecular triplet state He_2^* excimers on vortex lines has been studied by ballistic time-of-flight experiments.[6,20] This experiment demonstrates efficient trapping of He_2^* at low temperatures due to the attractive Bernoulli potential, which is $V_{IM-Vortex}(0) \approx -30$ K at 0 K. The ground atomic triplet state He^* appears less bound, $V(0) \approx -22$ K, due to its smaller bubble size occupied in the liquid. Both binding energy values decrease at finite temperatures as both a_F and $\rho_{s,0}$ are temperature dependent.

Most previous theoretical studies have expressed the solvation bubble size around impurities in terms of the mass barycenter position, R_b,[55,56]

$$\int_0^{R_b} \rho(R) d^3R = \int_{R_b}^{\infty} (\rho_0 - \rho(R))\, d^3R, \tag{9}$$

where ρ_0 corresponds to the bulk liquid density. This calculated radius is frequently found to be somewhat smaller than experimental estimates indicate. Consider, for example, the electron bubble (0 K temperature and saturated vapor pressure) for which OT-DFT calculations predict a bubble radius of $R_b \approx 18.5$ Å.[45] Experiments analyzing the electron–vortex trapping lifetime, which employ Eq. (4), give $R \approx 19.5$ Å,[59] (and in this work even larger $R \approx 22.2$ Å) and photoejection of electrons from the bubble yields $R \approx 21.2$ Å,[67] which both assume classical representation for the bubble interface with a sharp Heaviside wall appearing between the impurity and the liquid. It is not surprising that this classical radius is not necessarily equal to the barycenter radius as demonstrated in practice in Fig. 5 where the calculated 0 K OT-DFT liquid density profiles for He^*, He_2^*, and e^- are shown. In each case, the classical bubble size R points beyond the barycenter radius to the regime where the bulk density is approached. For example, for the electron, the difference between the barycenter and classical radius values is almost 3 Å. Hence, we conclude that the use of the classical interface profile results in a slight over estimation of the bubble radius as compared with the actual barycenter radius. While the latter is defined more exactly than the classical radius, it still remains ill-defined for impurities, which exhibit strong density oscillations in the bubble interface region.

If the external pressure is increased, the impurity bubble radius (i.e., R) decreases and, consequently, the impurity–vortex interaction becomes smaller according to Eq. (4) (see also Refs. 45 and 59). In principle, the value of a_F may also be affected by pressure but the vortex size variation is much smaller than, for example, for the electron

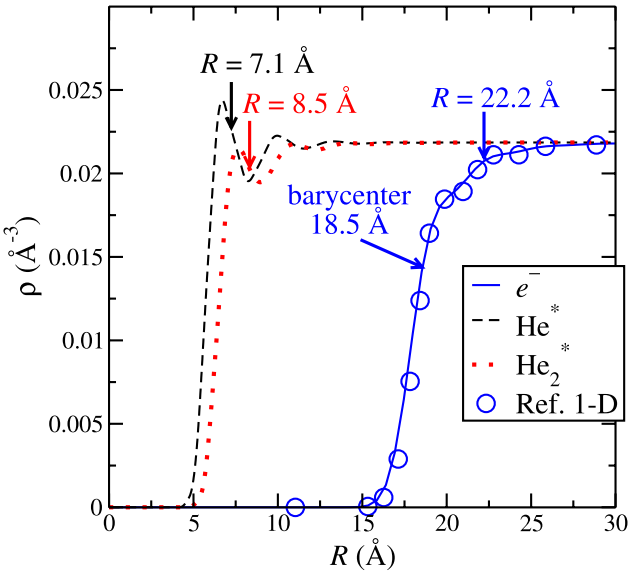

FIG. 5. Superfluid helium density profiles around e^-, He^*, and He_2^* impurities at 0 K. The arrows indicate the position of the effective radius R according to Eq. (4). The 1D reference data were taken from Ref. 45. The calculated barycenter radius using Eq. (9) for the electron is also indicated by an arrow.

bubble, and therefore, the pressure dependence in R dominates the overall energetics. This is demonstrated for the solvated electron in Fig. 6 where the bubble radius is strongly affected by pressure.[45] At 2.5 MPa, the binding energy decreases already down to −73 K, which predicts that it is possible to observe the thermally assisted electron escape process at lower temperatures when pressure is increased. Such experiments could help eliminate the uncertainties related to the temperature dependence present in a_F and $\rho_{0,s}$ when analyzing the experimental data. The behavior of the electron in the negative pressure regime was discussed in earlier work.[33] For all other impurities considered in this study, the effect of pressure is very small simply because they are much less

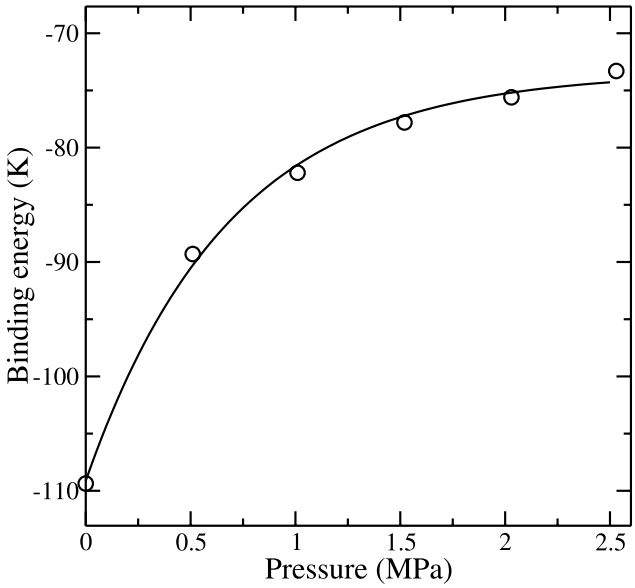

FIG. 6. Electron–vortex interaction energy at 0 K as a function of external pressure (open circles). The solid line is provided as a guide to the eye.

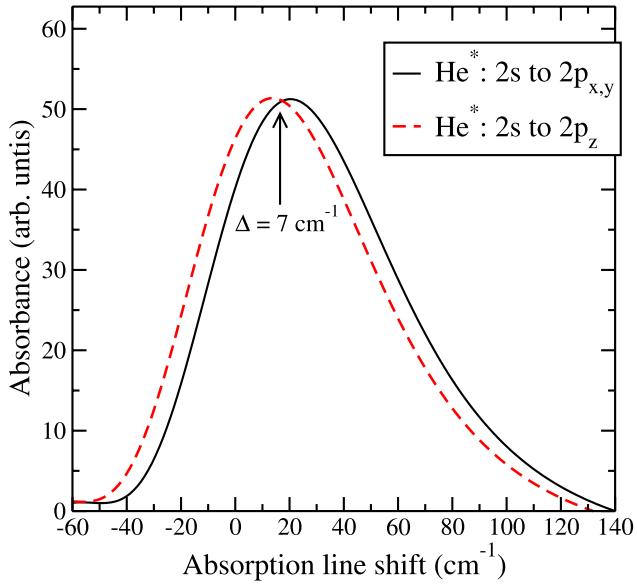

FIG. 7. Comparison between the optical absorption bands of He^* for the $2s-2p_{x,y}$ (perpendicular) and $2s-2p_z$ (parallel) transitions. A dephasing time of $\tau = 150$ fs was used to damp out the time-domain signal.[68] The gas phase origin on the x-axis is located at 0 cm^{-1}. The two bands are shifted from each other by the amount indicated with Δ.

compressible than the electron. For example, for He_2^* at 0 K, the change in the binding energy between the saturated vapor pressure and 2.5 MPa is only 0.5 K. The increase in bulk liquid density (cf. Eq. (4)) as a function of pressure would slightly counteract this reduction.

Finally, we consider a new scheme for identifying trapping of impurities at vortex lines through optical absorption spectroscopy. To demonstrate the concept, we consider the $2s$ to $2p$ electric dipole allowed transition of He^* in its triplet state electronic manifold. The resulting absorption spectrum in bulk superfluid helium has been recently modeled by computing the time-dependent response of the surrounding bath due to the change in the He^*–He interaction potential.[68] We use this approach to evaluate the absorption spectra of He^* in bulk vs. He^* trapped on a vortex line (saturated vapor pressure and 0 K). Since the upper state is a p-state, it is subject to Jahn-Teller splitting due to symmetry breaking induced by the vortex line. The absorption spectra corresponding to excitation from $2s$ to $2p_z$ (vortex line along z) and $2p_{\{x,y\}}$ (perpendicular to vortex line) are shown in Fig. 7. The latter transition produces nearly indistinguishable spectrum from bulk solvation ("bulk band") whereas the former red shifts by ca. 7 cm^{-1} ("vortex band"). Judging from the previous experimental measurement of this absorption line as a function of pressure, this shift should be large enough to be resolved.[69,70] Since He^* trapped on a vortex line yields both absorption bands overlapping, the measurement would produce a broad sum spectrum. To verify the presence of the vortex band, the bulk band should be subtracted out. This would require a reference measurement of He^* without vortex trapping. In practice, fluorescence spectroscopy is more sensitive than absorption and would offer advantages in visualization applications. However, although the spectra should also shift in a similar way, these shifts are typically smaller and it may not be possible to spectrally resolve these bands.

IV. CONCLUSIONS

We have obtained a new parametrization for describing the vortex core structure in superfluid helium at 0 K as represented by the effective healing length parameter a_F. The value found is very close to the result obtained from re-analyzing the Rayfield-Reif experiment. It is also consistent with the parameter values obtained from fitting the DFT derived potential data to the Donnelly-Parks (DP) function. The interaction between a rectilinear vortex line and a number of impurities has been computed, and the theoretical model was validated against the known experimental data for the electron and positive ion. For the electron, thermal corrections to the vortex binding energy are large and had to be included in theoretical values to produce results in agreement with the experimental data. The binding energies of small atoms and molecules on quantized vortex lines are significant, of order of tens of Kelvin, and therefore vortices act as efficient traps for such impurities at low temperatures. Based on the extrapolation of the 0 K DFT data, vortex lines present permanent traps for larger nanometer scale objects in the superfluid phase, if the effects of vortex motion can be minimized by using a large cell or adding ^{3}He. This has important applications for visualizing vortex lines by light scattering and absorption (i.e., shadowgraph imaging). Finally, a new scheme for identifying impurity trapping at vortex lines is outlined based on the helium-induced optical absorption band shifts. For He^*, the vortex-induced band shift was shown to be large enough compared with the resolution obtained in previous experiments, which suggests that it is possible to observe this effect experimentally.

ACKNOWLEDGMENTS

Financial support from the National Science Foundation Grant Nos. CHE-1262306 and DMR-1205734 and the Interdisciplinary Research Institute for the Sciences (IRIS) is gratefully acknowledged.

[1]G. Careri, W. D. McCormick, and F. Scaramuzzi, Phys. Lett. **1**, 61 (1962).
[2]R. L. Douglass, Phys. Rev. Lett. **13**, 791 (1964).
[3]R. L. Douglass, Phys. Rev. **174**, 255 (1968).
[4]W. I. Glaberson, D. M. Strayer, and R. J. Donnelly, Phys. Rev. Lett. **20**, 1428 (1968).
[5]R. M. Ostermeier and W. I. Glaberson, Phys. Rev. Lett. **35**, 241 (1975).
[6]D. E. Zmeev, F. Pakpour, P. M. Walmsley, A. I. Golov, W. Guo, D. N. McKinsey, G. G. Ihas, P. V. E. McClintock, S. N. Fisher, and W. F. Vinen, Phys. Rev. Lett. **110**, 175303 (2013).
[7]R. M. Ostermeier and W. I. Glaberson, J. Low Temp. Phys. **20**, 159 (1975).
[8]A. G. Cade, Phys. Rev. Lett. **15**, 238 (1965).
[9]G. A. Williams, K. DeConde, and R. E. Packard, Phys. Rev. Lett. **34**, 924 (1975).
[10]R. M. Ostermeier and W. I. Glaberson, Phys. Lett. A **51**, 348 (1975).
[11]G. A. Williams and R. E. Packard, Phys. Rev. Lett. **33**, 280 (1974).
[12]G. P. Bewley, D. P. Lathrop, and K. R. Sreenivasan, Nature **441**, 588 (2006).
[13]G. A. Williams and R. E. Packard, Phys. Rev. Lett. **35**, 237 (1975).
[14]G. A. Williams and R. E. Packard, J. Low Temp. Phys. **23**, 459 (1978).
[15]E. Popov, M. Mammetkuliyev, and J. Eloranta, J. Chem. Phys. **138**, 204307 (2013).

[16]E. B. Gordon, A. V. Karabulin, V. I. Matyushenko, V. D. Sizov, and I. I. Khodos, Chem. Phys. Lett. **519-520**, 64 (2012).
[17]A. F. Borghesani, *Ions and Electrons in Liquid Helium* (Oxford Science Publications, New York, 2007).
[18]R. J. Donnelly and P. H. Roberts, Proc. R. Soc. A **312**, 519 (1969).
[19]G. A. Williams and R. E. Packard, J. Low Temp. Phys. **39**, 353 (1980).
[20]W. Guo, S. B. Cahn, J. A. Nikkel, W. F. Vinen, and D. N. McKinsey, Phys. Rev. Lett. **105**, 045301 (2010).
[21]D. Meichle and D. Lathrop, Rev. Sci. Instrum. **85**, 073705 (2014).
[22]E. Fonda, D. Meichle, N. Ouellette, S. Hormoz, and D. Lathrop, Proc. Natl. Acad. Sci. U. S. A. **111**(Suppl. 1), 4707 (2014).
[23]E. B. Gordon, Low Temp. Phys. **38**, 1043 (2012).
[24]E. B. Gordon, A. V. Karabulin, V. I. Matyushenko, V. D. Sizov, and I. I. Khodos, Appl. Phys. Lett. **101**, 052605 (2012).
[25]E. B. Gordon, A. V. Karabulin, V. I. Matyushenko, V. D. Sizov, and I. I. Khodos, J. Exp. Theor. Phys. **112**, 1061 (2011).
[26]E. Gordon, A. Karabulin, V. Matyushenko, V. Sizov, and I. Khodos, Phys. Chem. Chem. Phys. **16**, 25229 (2014).
[27]L. F. Gomez, E. Loginov, and A. F. Vilesov, Phys. Rev. Let. **108**, 155302 (2012).
[28]D. Spence, E. Latimer, C. Feng, A. Boatwright, A. M. Ellis, and S. Yang, Phys. Chem. Chem. Phys. **16**, 6903 (2014).
[29]E. Latimer, D. Spence, C. Feng, A. Boatwright, A. M. Ellis, and S. Yang, Nano Lett. **14**, 2902 (2014).
[30]P. Thaler, A. Volk, F. Lackner, J. Steurer, D. Knez, W. Grogger, F. Hofer, and W. E. Ernst, Phys. Rev. B **90**, 155442 (2014).
[31]N. G. Berloff and P. H. Roberts, Phys. Rev. B **63**, 024510 (2000).
[32]P. E. Parks and R. J. Donnelly, Phys. Rev. Lett. **16**, 45 (1966).
[33]M. Pi, R. Mayol, A. Hernando, M. Barranco, and F. Ancilotto, J. Chem. Phys. **126**, 244502 (2007).
[34]A. L. Fetter, Phys. Rev. Lett. **27**, 986 (1971).
[35]P. H. Roberts and R. J. Donnelly, Phys. Lett. A **31**, 137 (1970).
[36]C. F. Barenghi, R. J. Donnelly, and W. F. Vinen, J. Low Temp. Phys. **52**, 189 (1983).
[37]G. W. Rayfield and F. Reif, Phys. Rev. **136**, A1194 (1964).
[38]W. L. Glaberson and M. Steingart, Phys. Rev. Lett. **26**, 1423 (1971).
[39]W. I. Glaberson and R. J. Donnelly, *Structure, distributions and dynamics of vortices in helium II* in Progress in Low Temperature Physics, edited by D. F. Brewer (Elsevier Science Publishers, 1986), Vol. 9.
[40]J. Wilks, *The Properties of Liquid and Solid Helium* (Clarendon Press, Oxford, 1967).
[41]R. P. Henkel, E. N. Smith, and J. D. Reppy, Phys. Rev. Lett. **23**, 1287 (1969).
[42]F. Dalfovo, A. Lastri, L. Pricaupenko, S. Stringari, and J. Treiner, Phys. Rev. B **52**, 1193 (1995).
[43]L. Lehtovaara, T. Kiljunen, and J. Eloranta, J. Comput. Phys. **194**, 78 (2004).
[44]L. Lehtovaara, J. Toivanen, and J. Eloranta, J. Comput. Phys. **221**, 148 (2007).
[45]J. Eloranta and V. A. Apkarian, J. Chem. Phys. **117**, 10139 (2002).
[46]J. Eloranta and V. A. Apkarian, J. Chem. Phys. **115**, 752 (2001).
[47]N. Bonifaci, F. Aitken, V. M. Atrazhev, S. L. Fiedler, and J. Eloranta, Phys. Rev. A **85**, 042706 (2012).
[48]J. Jortner, N. R. Kestner, S. A. Rice, and M. H. Cohen, J. Chem. Phys. **43**, 2614 (1965).
[49]J. J. Moré, B. S. G., and K. E. Hillstrom, "User guide for MINPACK-1," ANL-80-74, Argonne National Laboratory, 1980.
[50]E. Sola, J. Casulleras, and J. Boronat, Phys. Rev. B **76**, 052507 (2007).
[51]G. Ortiz and D. M. Ceperley, Phys. Rev. Lett. **75**, 4642 (1995).
[52]D. E. Galli, L. Reatto, and M. Rossi, Phys. Rev. B **89**, 224516 (2014).
[53]F. Dalfovo, Phys. Rev. B **46**, 5482 (1992).
[54]F. Dalfovo, R. Mayol, M. Pi, and M. Barranco, Phys. Rev. Lett. **85**, 1028 (2000).
[55]J. Eloranta, N. Schwentner, and V. A. Apkarian, J. Chem. Phys. **116**, 4039 (2002).
[56]D. Mateo and J. Eloranta, J. Phys. Chem. A **118**, 6407 (2014).
[57]K. R. Atkins, Phys. Rev. **116**, 1339 (1959).
[58]S. T. Hannahs and G. A. Williams, Phys. Rev. B **42**, 7901 (1990).
[59]J. W. P. Pratt and J. W. Zimmermann, Phys. Rev. **177**, 412 (1969).
[60]K. DeConde, G. A. Williams, and R. E. Packard, Phys. Rev. Lett. **33**, 683 (1974).
[61]V. Grau, M. Barranco, R. Mayol, and M. Pi, Phys. Rev. B **73**, 064502 (2006).
[62]F. Ancilotto, F. Faccin, and F. Toigo, Phys. Rev. B **62**, 17035 (2000).
[63]T. Padmore, Phys. Rev. Lett. **28**, 469 (1972).
[64]P. Walmsley, A. Golov, A. Levchenko, and B. White, J. Low Temp. Phys. **148**, 317 (2007).
[65]R. Mayol, M. Pi, M. Barranco, and F. Dalfovo, Phys. Rev. Lett. **87**, 145301 (2001).
[66]Y. Sergeev and C. Barenghi, J. Low Temp. Phys. **157**, 429 (2009).
[67]J. A. Northby and T. M. Sanders, Phys. Rev. Lett. **18**, 1184 (1967).
[68]S. L. Fiedler and J. Eloranta, J. Low Temp. Phys. **174**, 269 (2014).
[69]A. P. Hickman and N. F. Lane, Phys. Rev. B **12**, 3705 (1975).
[70]F. J. Soley and W. A. Fitzsimmons, Phys. Rev. Lett. **32**, 988 (1974).